Published in final edited form as:
Cancer Discov. 2014 June ; 4(6): 716–729. doi:10.1158/2159-8290.CD-13-0743.

p38MAPK plays a crucial role in stromal mediated tumorigenesis

Elise Alspach[1,2], **Kevin C. Flanagan**[1,2], **Xianmin Luo**[1,2], **Megan K. Ruhland**[1,2], **Hui Huang**[1,2], **Ermira Pazolli**[1,*], **Maureen J. Donlin**[5], **Timothy Marsh**[6], **David Piwnica-Worms**[**], **Joseph Monahan**[7], **Deborah V. Novack**[3,4], **Sandra S. McAllister**[6,8], and **Sheila A. Stewart**[1,2,3]

[1]Department of Cell Biology and Physiology, Washington University School of Medicine, St. Louis, MO 63110

[2]BRIGHT Institute, Washington University School of Medicine, St. Louis, MO 63110

[3]Department of Medicine, Washington University School of Medicine, St. Louis, MO 63110

[4]Department of Pathology and Immunology, Washington University School of Medicine, St. Louis, MO 63110

[5]Departments of Biochemistry & Molecular Biology and of Molecular Microbiology & Immunology, Saint Louis University School of Medicine, St. Louis, MO 63103

[6]Hematology Division, Department of Medicine, Brigham and Women's Hospital, Harvard Medical School, Boston, MA 02115

[7]Confluence Life Sciences Inc., St. Louis, MO, 63108

[8]Harvard Stem Cell Institute and Broad Institute of Harvard and MIT, Cambridge, MA, 02138

Abstract

Neoplastic cells rely on the tumor microenvironment (TME) for survival and progression factors. Indeed, senescent and cancer-associated fibroblasts (CAFs) express factors that promote tumorigenesis that are collectively referred to as the senescence-associated secretory phenotype (SASP). Despite their importance in tumorigenesis, the mechanisms that control TME-derived factor expression remain poorly understood. Here we address a key unanswered question, how the SASP is sustained in senescent fibroblasts and CAFs. We find that the mitogen-activated protein kinase p38 (p38MAPK) controls AUF1 occupancy on SASP mRNAs and thus controls their stability. The importance of this regulatory mechanism is underscored by our findings that stromal-specific p38MAPK inhibition abrogates the tumor-promoting activities of CAFs and senescent fibroblasts. Our data suggest that targeting SASP mRNA stability through inhibition of p38MAPK will significantly aid the development of clinical strategies to target the TME.

Corresponding Author: Sheila A. Stewart, Department of Cell Biology and Physiology, Washington University School of Medicine, 660 South Euclid Avenue, Campus Box 8228, St. Louis, MO 63110. Phone: 314-362-7437; Fax: 314-362-7463; sheila.stewart@wustl.edu.
*Current address: AstraZeneca Pharmaceuticals, Waltham, MA.
**Current address: Department of Cancer Systems Imaging, MD Anderson Cancer Center, Houston, TX.

Conflict of Interest: None

Keywords

tumor microenvironment; senescence; SASP; mRNA stability; p38MAPK

INTRODUCTION

The critical role the tumor microenvironment (TME) plays in disease is underscored by findings that changes within stromal cells can predict clinical outcome (1) (2) (3). For this reason, many groups have focused on how various stromal cell types impact tumorigenesis. For example, activated fibroblasts isolated from carcinomas (cancer-associated fibroblasts or CAFs) promote preneoplastic cell growth and increase tumor cell migration, invasion, and angiogenesis (4). Likewise, senescent fibroblasts, which are also found in human tissue (5), support tumorigenesis through the promotion of growth, invasion, and angiogenesis (6) (7) (8). Intriguingly, both senescent fibroblasts and CAFs express a plethora of pro-tumorigenic factors and in senescent cells this is referred to as the senescence-associated secretory phenotype (SASP) (6) (9).

There is significant overlap between the pro-tumorigenic factors expressed in CAFs and senescent cells. Expression array analyses of human fibroblasts treated with granulin, which renders a CAF-like phenotype (10), and fibroblasts isolated from human tumors reveal that both populations express SASP factors ((11) (12) and reviewed in (13)). In addition, CAFs isolated by laser capture micro-dissection (LCM) or via cell surface marker expression similarly display SASP factor expression (1) (2) (3) (4) (14). Finally, cells that fail to enter senescence following exposure to a senescence-inducing stress robustly express SASP factors (15) (16), indicating that entrance into senescence is not a prerequisite for SASP expression. Together, these observations raise the possibility that the mechanisms that govern SASP expression are conserved in many tumor-promoting fibroblasts and are not dependent upon the induction of senescence. Thus, identifying mechanisms that activate and sustain SASP expression will have a profound impact on our understanding of the development of a pro-tumorigenic TME and the identification of novel therapeutic targets.

Despite the profound impact the pro-tumorigenic SASP has on tumor cell growth and progression, the mechanisms that lead to its activation and maintenance remain poorly understood. The majority of regulatory pathways elucidated thus far have focused on SASP factor transcription, specifically by NFκB and C/EBPβ (15) (16) (17) (18) (19). NFκB's transcriptional activation of the SASP is dependent on the mitogen-activated protein kinase p38 (p38MAPK) and the DNA-damage response protein ATM (19). However, in other systems p38MAPK facilitates expression of cytokines including IL6 by impacting post-transcriptional mRNA stability, possibly through the RNA binding-protein AUF1 (20) (21) (22). Post-transcriptional regulation of the SASP by p38MAPK has yet to be investigated.

Given the importance of the SASP on stromal-supported tumorigenesis, we investigated the impact of p38MAPK on SASP-mediated tumor promotion. We demonstrate that inhibition of p38MAPK activity abrogates the tumor promoting capacity of senescent fibroblasts. Furthermore, inhibiting p38MAPK in CAFs inhibits their tumor promoting abilities, demonstrating for the first time that regulatory mechanisms elucidated in senescent stroma

are applicable in CAFs. Finally, we elucidate a p38MAPK-dependent post-transcriptional SASP regulatory pathway that modulates RNA-binding protein activity.

RESULTS

p38MAPK activity controls the pro-tumorigenic properties of the SASP

SASP factors promote preneoplastic cell growth (6) (7) (8) (23) (24) and p38MAPK contributes significantly to the initiation of SASP factor expression (25). To confirm this, senescent fibroblasts (fibroblasts staining positive for senescence-associated β-gal, SA-β-gal, Supplemental Fig. 1A) were treated with a highly specific small-molecule inhibitor of p38MAPK (SB203580) (26). Hsp27 is a direct downstream target of p38MAPK. Therefore, to confirm that our treatment inhibited the kinase activity of p38MAPK, we measured Hsp27 phosphorylation by western blot analysis. We found that SB203580 treatment led to a reduction in Hsp27 phosphorylation, indicating successful inhibition of p38MAPK activity (Fig. 1A). As expected, SB203580 treatment of senescent fibroblasts resulted in a significant reduction in the expression of SASP factors IL6, IL8, and GMCSF (Fig. 1B). To determine if p38MAPK activity was responsible for the tumor-promoting activities of senescent cells, we performed co-culture experiments with normal human fibroblasts induced to senesce by treatment with bleomycin (referred to throughout as stress-induced premature senescence, SIPS) and preneoplastic HaCaT keratinocyte cells expressing click beetle red (CBR) luciferase (HaCaT-CBR) (23). Prior to the addition of HaCAT-CBR cells, fibroblasts were treated with vehicle or SB203580 as indicated in Fig. 1C. Senescent fibroblasts treated with vehicle increased the growth of HaCaT-CBR cells compared to HaCaT-CBR cells cultured with young fibroblasts (Fig. 1D), recapitulating our previously published observations (23) (15). However, while inhibition of p38MAPK had no effect on HaCAT-CBR cells grown in the absence of fibroblasts (Supplemental Fig. 1B), we found that p38MAPK inhibition reduced the pro-tumorigenic activity of senescent fibroblasts by significantly reducing HaCaT-CBR cell growth (Fig. 1D).

Given the potent impact of p38MAPK inhibition in co-culture experiments, we next examined the impact of p38MAPK depletion on preneoplastic cell growth in xenograft experiments. p38MAPK was depleted from senescent fibroblasts (Fig. 1E), resulting in a significant reduction in the level of p38MAPK-dependent SASP factor IL8 (Fig. 1F). To assess the impact of p38MAPK loss in vivo, young, senescent, or p38MAPK-depleted senescent fibroblasts were admixed with the preneoplastic epithelial cell line BPH1 expressing CBR luciferase (BPH1-CBR) and injected subcutaneously into nude mice. Tumor growth was analyzed by bioluminescence imaging. As expected, senescent fibroblasts increased BPH1-CBR cell growth relative to young fibroblasts (Fig. 1G). However, depletion of p38MAPK and subsequent reduction in p38MAPK-dependent SASP factor expression reduced tumor growth to the level observed when BPH1-CBR cells were co-injected with young fibroblasts (Fig. 1G). These results indicate that expression of p38MAPK-dependent SASP factors within the TME plays a pivotal role in preneoplastic cell growth in vivo.

The pro-tumorigenic SASP is subject to post-transcriptional regulation

We next sought to elucidate the mechanism by which p38MAPK regulates pro-tumorigenic SASP factor expression. Previous work demonstrated that p38MAPK modulates NFκB-driven transcription of SASP factors including IL6 and IL8 (19). To determine that the effects of p38MAPK inhibition were transcriptionally based, senescent fibroblasts were treated with the transcription inhibitor actinomycin D (ActD) at several time points following bleomycin treatment. SASP factor expression was significantly inhibited when cells were treated with ActD 24 hours after bleomycin treatment (Fig. 2A), a time point at which SASP factor mRNA was increased (Supplemental Fig. 2A) but cells were not yet senescent (Supplemental Fig. 1A). These results indicate that at this time point SASP factor expression is dependent on transcription. Surprisingly, at 96 hours after bleomycin treatment, when cells displayed morphological features characteristic of senescence including staining positive for SA-β-gal (Supplemental Fig. 1A), treatment with ActD failed to reduce SASP factor mRNA levels (Fig. 2A). These changes in mRNA were also reflected at the protein level. Indeed, we found that IL6 protein levels in conditioned medium collected from cells treated with ActD at 24 hours fell drastically compared to untreated cells. In contrast, when cells were treated with ActD at 96 hours, IL6 protein levels remained high (Fig. 2B). Given p38MAPK inhibition at the later time point significantly reduced SASP expression (Fig. 1B), these findings raised the possibility that p38MAPK impacts SASP factor mRNA stability rather than NFκB-driven transcriptional activation upon the acquisition of senescence. To confirm that p38MAPK had no effect on NFκB-driven transcription at the later time point, normal human fibroblasts were transduced with an NFκB transcription reporter plasmid driving expression of luciferase (NFκB-luc). Transduced cells were treated with bleomycin, and 72 hours later senescent cells were treated with the p38MAPK inhibitor SB203580 for an additional 48 hours. As expected, when SB203580 treatment was initiated 72 hours after bleomycin treatment, there was no significant effect on NFκB transcriptional activity (Fig. 2C). These results indicate that after the establishment of senescence, p38MAPK has a profound effect on SASP factor mRNA stability.

To address whether SASP factor mRNA stability was affected in cells undergoing replicative senescence or other types of stress-induced senescence, normal human fibroblasts were induced to senesce through telomere dysfunction (replicative senescence, RS) or treatment with the histone deacetylase inhibitor sodium butyrate (NaB). Cells undergoing RS or NaB-induced senescence robustly induced expression of SASP factors, including IL6 and IL8 (Supplemental Fig 2B and Supplemental Fig 2C, **respectively**). Further, we found that SASP factor mRNAs were significantly stabilized in cells that had undergone RS or NaB-induced senescence (Fig. 2D **and** Supplemental Fig. 2D, **respectively**). Significantly, SASP factor mRNA stabilization was not limited to skin fibroblasts; when IMR90 human lung fibroblasts were treated with bleomycin, they displayed a similar increase in SASP factor mRNA stability 96 hours post-bleomycin treatment (Supplemental Fig. 2E). Together, these data indicate that SASP factor mRNAs are stabilized by a post-transcriptional regulatory program that is active in fibroblasts from diverse tissues, regardless of the mechanism through which senescence is induced.

p38MAPK post-transcriptionally regulates the SASP

Our results indicate that p38MAPK inhibition reduces SASP expression and TME-dependent promotion of tumorigenesis but does not affect the activity of the primary transcriptional regulator of the SASP, NFκB, following induction of senescence. Interestingly, p38MAPK post-transcriptionally regulates IL6 and IL8 in other contexts (20) (21). Thus, we investigated p38MAPK's role in stabilizing SASP factor mRNA. We first examined whether p38MAPK was active throughout the time course under investigation. To assess p38MAPK activation, lysates were prepared from cells 24 or 96 hours after bleomycin treatment and examined for phosphorylated p38MAPK (p-p38) by western blot analysis. In agreement with previous findings (19), we observed that phosphorylated p38MAPK increased from 24 to 96 hours following bleomycin treatment (Supplemental Fig. 2F). These kinetics were consistent with SASP factor mRNA stabilization, suggesting that p38MAPK activation regulates SASP factor mRNA stability.

To elucidate p38MAPK's role in regulating SASP factor mRNA stabilization, normal human fibroblasts depleted of p38MAPK (shp38) were treated with ActD 24 or 96 hours after bleomycin treatment (Fig. 2E). When treated with ActD 24 hours after bleomycin treatment, cells expressing shSCR or shp38 displayed decreased SASP mRNA stability, indicating that p38MAPK does not post-transcriptionally regulate SASP mRNAs at this time point. As expected, both IL6 and IL8 mRNA stability increased when shSCR control cells were treated with ActD 96 hours after bleomycin treatment, although not to the same extent as that observed in non-transduced fibroblasts. In contrast, when shp38 cells were treated with ActD 96 hours post-bleomycin treatment, they displayed significantly reduced IL6 and IL8 mRNA stability when compared to cells expressing the control hairpin (shSCR) (Fig. 2E). Similar results were obtained with a second independent shRNA targeting p38MAPK (data not shown).

The 3' UTRs of SASP factor transcripts control mRNA stabilization in stromal cells

We next examined the mechanisms by which SASP factor mRNA was stabilized. The 3' untranslated region (UTR) of many mRNAs contains protein binding motifs that alter mRNA stability under diverse biological stimuli (27). To determine whether the 3' UTRs of SASP factor mRNAs govern post-transcriptional regulation, we utilized a luciferase reporter cDNA fused to the 3' UTR of IL6 (lucIL6) or GMCSF (lucGMCSF). A luciferase reporter cDNA fused to the 3' UTR of GAPDH (lucGAP) was used as a control. Normal human fibroblasts were stably transduced with the luciferase reporter constructs and luciferase mRNA levels were monitored in response to ActD at the time points indicated (Fig. 3A). Similar to our observations with the endogenous IL6 and GMCSF transcripts, we observed that the stability of the lucIL6 and lucGMCSF transcripts increased significantly when treated with ActD 96 hours compared to 24 hours after bleomycin treatment (Fig. 3A). As expected, there was no significant change in the stability of the lucGAP transcript (Fig. 3A), indicating that 3' UTR-dependent mRNA stabilization was specific for SASP factor mRNA and did not extend to all mRNAs in response to senescence. These results indicate that the 3' UTR of SASP factor transcripts mediates increases in mRNA stability.

AUF1 directly binds to SASP factor mRNA and modulates their stabilization

AUF1 is a protein that binds the 3' UTRs of many mRNAs including IL6, IL8, and GMCSF and reduces their stability (28) (29) (30). Furthermore, p38MAPK is known to impact AUF1 activity in other settings (22), although a link between AUF1 and p38MAPK in the post-transcriptional regulation of IL6 and IL8 has not been demonstrated. To examine AUF1 binding to SASP factor mRNA in response to senescence, we utilized RNA-binding protein immunoprecipitation (RIP) to examine AUF1 binding to SASP factor mRNAs in response to senescence. Cell lysates were collected 24 and 96 hours after bleomycin treatment and subjected to immunoprecipitation with either an AUF1-specific antibody or a nonspecific IgG; mRNA levels were normalized to the levels of each transcript measured in the input fractions. We observed that AUF1 occupancy on IL6 and IL8 mRNAs significantly decreased from 24 to 96 hours after bleomycin treatment (Fig. 3B), corresponding with the increase in mRNA stability observed in Fig. 2. We observed similar results for GMCSF and CCL20 mRNA, indicating that this mechanism impacts many SASP factor mRNAs (Fig. 3B). This observation suggests that decreased AUF1 binding leads to increased mRNA stability once senescence is established.

We next sought to determine whether AUF1 was required to destabilize SASP mRNAs. To address this question, we stably transduced normal human fibroblasts with two independent short-hairpin RNA (shRNA) constructs targeting AUF1 (shAUF1a and shAUF1b) (Fig. 3C). AUF1-depleted cells were treated with bleomycin and 24 hours later treated with ActD, a time at which AUF1 is bound to SASP factor mRNAs displaying reduced stability (Fig. 3B). In contrast to control cells, we found that AUF1 depletion significantly increased the stability of IL6 and IL8 mRNA at the early time point when these mRNAs are normally unstable (Fig. 3D). These data demonstrate that before senescence is established, AUF1 destabilizes SASP mRNAs by binding to their 3' UTRs.

To address whether the impact of p38MAPK on SASP mRNA stabilization was due to modulation of AUF1–SASP mRNA binding, we carried out RIP analysis. Following bleomycin treatment, normal human fibroblasts were treated with SB203580 or vehicle control as described in Fig. 3E. In contrast to control cells in which AUF1 occupancy decreased at the late time point, there was no decrease in AUF1 occupancy on IL8 mRNA in p38MAPK-inhibited cells collected 96 hours after bleomycin treatment (Fig. 3E). Similar results were obtained for IL6 (data not shown). These observations indicate that p38MAPK activation is required to release AUF1 from SASP factor mRNA. Further, these studies suggest that loss of SASP factor mRNA stabilization in p38MAPK inhibited cells (Fig. 2) is the result of a failure to remove AUF1 from SASP factor transcripts.

p38MAPK-dependent factors are expressed in the TME of breast cancer lesions

The TME plays a pivotal role in tumor progression, and recent expression analyses indicate that TME-specific expression changes are predictive of clinical outcome (1) (2) (3). Both senescent fibroblasts and CAFs express pro-tumorigenic SASP factors, raising the intriguing possibility that the regulatory mechanisms that control SASP expression in senescent cells also operate in cancer-associated stroma. Given the importance of p38MAPK in SASP factor expression, we carried out a meta-analysis to establish a list of p38MAPK-regulated

genes in senescent fibroblasts and evaluated their expression in the TME of human breast cancers (Fig. 4A). We performed RNA sequence analysis (RNA-seq) of young, senescent, and p38MAPK-inhibited senescent human fibroblasts and observed that IL6 and IL8 expression was p38MAPK-dependent. Along with previously identified factors, we found that 50 additional SASP factors were p38MAPK-dependent, including GMCSF, GCSF, IL1α, IL1β, CXCL1, CXCL2, CXCL5, CCL20, MMP1, and MMP7 (Supplemental Table 1, Fig. 4A). A subset of these factors was validated by qRT-PCR (Supplemental Fig. 3A). Gene ontology (GO) process analysis performed on the p38MAPK-dependent factors demonstrated that genes related to the regulation of inflammation, chemotaxis, cell adhesion, angiogenesis, and proliferation were significantly enriched in this gene set (Fig. 4B).

We next compared our p38MAPK-dependent SASP list to factors significantly over-expressed in the TME of breast cancer (BC) lesions. We examined three data sets generated from microarray analyses of normal stroma versus cancer-associated stroma that had been obtained by laser capture micro-dissection of breast tissue (1) (2) (3) (Fig. 4A). Of the 50 p38MAPK-dependent factors identified in senescent fibroblasts, we found that 29 were expressed in the stroma of the Finak breast cancer dataset (1), including CXCL2 and IL24. Seventeen factors were expressed in the TME of the Ma breast cancer data set (2), including IL1β. Finally, 7 factors overlapped with the Karnoub breast cancer data set (3), including CCL20 (Supplemental Table 1). Furthermore, CCL20, CXCL5, IL11, IL1β, IRAK3, MMP1, MPP7, and SOD2 were expressed in the BC-associated stromal compartment of at least two studies (Fig. 4C). Of note, CCL20, CXCL5, IL11, IL1β, and MMP1 are factors with known pro-tumorigenic activities (31) (32) (33) (34) (35). We observed that BC-associated stromal genes compose a large percentage of the total number of p38MAPK-dependent SASP factors involved in the regulation of inflammation, chemotaxis, angiogenesis, and cell adhesion based on GO process analyses (Fig. 4B). Given that these factors are associated with disease progression, our findings raise the possibility that anti-p38MAPK therapy could significantly impact tumor progression in humans.

Inhibition of p38MAPK abrogates the pro-tumorigenic activities of CAFs

Expression of p38MAPK-dependent factors within the stroma of breast cancer lesions raised the possibility that they contribute to the tumor promoting activities of CAFs. Therefore, we examined whether inhibition of p38MAPK would abrogate the tumor-promoting activities of CAFs as it did for senescent fibroblasts. To generate CAFs, we obtained normal human mammary fibroblasts from reduction mammoplasty (NMF), admixed them with MCF7-Ras breast carcinoma cells and injected the cell mixture into immunocompromised mice and allowed tumors to grow. Human CAFs were isolated from these tumors and we assessed their tumor-promoting potential by co-culturing them with preneoplastic HaCaT skin keratinocytes expressing CBR luciferase (HaCaT-CBR). As expected, CAFs significantly stimulated HaCaT-CBR cell growth compared to HaCaT-CBR cells cultured with parental NMF fibroblasts (Fig. 4D). To investigate the importance of p38MAPK-dependent CAF factors, we inhibited p38MAPK in CAFs with SB203580 and assessed their ability to promote preneoplastic cell growth. Similar to what we observed when senescent fibroblasts were treated with the p38MAPK inhibitor SB203580 (Fig. 1C), CAFs treated with

SB203580 failed to promote HaCaT-CBR cell growth (Fig. 4D). These results indicate that p38MAPK regulates the tumor-promoting activity of CAFs. Together with our meta-analysis and expression of p38MAPK-dependent genes in the stromal compartment of human breast cancer lesions, these observations suggest that p38MAPK plays a central role in sustaining the expression of tumor-promoting factors. Thus, stromal p38MAPK represents a novel therapeutic target for senescent and non-senescent cancer-associated stromal compartments in breast cancer.

p38MAPK inhibition compromises the tumor-promoting capacity of the microenvironment

The critical importance of SASP factor expression in our tumor models and our work to uncover the mechanisms that sustain SASP factor expression identified p38MAPK as a central player in SASP expression in senescent cells as well as in CAFs. Given our findings that p38MAPK-dependent factors are expressed in human breast cancer lesions, we evaluated the feasibility of targeting p38MAPK in a preventative and therapeutic setting. Several p38MAPK inhibitors have entered phase II clinical trails for rheumatoid arthritis and thus have proven safe in a nonlethal disease (36) (37). We obtained a p38MAPK inhibitor (CDD-111, also referred to as SD-0006 (38), Confluence Life Sciences) and compounded it into mouse chow. CDD-111 was chosen because it can be orally administered and shows high specificity for the p38MAPK α subunit (38). Indeed, extensive analysis of CDD-111 revealed that it is selective for p38MAPK α over fifty other kinases including p38MAPK β, γ, and δ. Furthermore, the IC_{50} for inhibiting tumor necrosis factor-α (TNFα) release in vitro and in vivo was less than 200 nM (38). Treatment of senescent cells with CDD-111 in vitro revealed that it effectively reduced SASP expression as evidenced by a significant reduction in IL6 and IL8 levels (data not shown).

To establish the impact of orally administered CDD-111 on p38MAPK activity in our system, mice were placed on CDD-111 (p38i) or control chow for three days, challenged with LPS, and serum TNFα levels were measured. We found that mice receiving oral p38i failed to mount a robust TNFα response following an LPS challenge compared to animals receiving control chow (Supplemental Fig. 3B). We also verified that p38i inhibited SASP expression in vivo. Senescent normal human fibroblasts were injected subcutaneously into the rear flanks of nude mice maintained on control or p38i chow. Ten days after injection the cells were removed, RNA was isolated, and the levels of human IL8 were analyzed by qRT-PCR. Senescent fibroblasts isolated from mice on p38i had significantly less IL8 mRNA than senescent fibroblasts isolated from mice on control chow (Fig. 4E), demonstrating that CDD-111 inhibited SASP expression in vivo.

We next evaluated the p38MAPK inhibitor's efficacy in a xenograft setting. BPH1-CBR cells admixed with young or senescent fibroblasts were subcutaneously injected into mice maintained on control or p38i chow (Fig. 4F). Bioluminescence analysis of tumor growth revealed that p38i significantly reduced the growth of BPH1-CBR cells co-injected with senescent fibroblasts (Fig. 4G & H). Analysis of cellular proliferation (Ki67 staining) revealed that senescent fibroblasts significantly increased BPH1 cell proliferation compared to when BPH1 cells were co-injected with young fibroblasts (Fig. 5A). Importantly, the increase BPH1 proliferation that was noted in the presence of senescent fibroblasts was

markedly reduced when mice were maintained on p38i versus control chow (Fig. 5A). These data demonstrate that the reduced tumor size observed in response to p38i administration was a result of decreased epithelial cell proliferation. Importantly, the difference in epithelial cell proliferation between tumors containing senescent stroma from p38i- and control-fed mice was not due to differences in stromal composition between these tumor types, as staining for a senescence marker, p16, and a fibroblast marker, vimentin, demonstrated that 1) senescent fibroblasts persisted throughout the time course of the experiment regardless of p38MAPK inhibition and 2) the stromal composition of treated and untreated tumors was similar. Vascularity and myeloid infiltration were also investigated in these tumors. No significant differences in either vascularity or leukocyte infiltration were noted (data not shown). Administration of CDD-111 to mice injected with BPH1 cells admixed with young fibroblasts also resulted in a decrease in epithelial cell growth, although not to the same extent as that observed in tumors containing senescent fibroblasts. Oral administration of CDD-111 had no significant impact on BPH1-CBR cells injected alone (data not shown).

To address the effectiveness of p38MAPK inhibition in a therapeutic setting, mice were injected with BPH1-CBR cells admixed with senescent fibroblasts and tumors were allowed to grow for one week until the average tumor volume reached 74 mm^3. Mice were then administered control or p38i chow and bioluminescence imaging was used to monitor tumor growth. Significantly, tumor growth was arrested in mice receiving p38i. In contrast, tumors in mice receiving control chow continued to show significant growth (Fig. 5B).

To investigate the applicability of orally administered p38i in CAF-containing microenvironments, we obtained primary CAFs (pCAFs) from a lesion removed from a patient with invasive breast cancer. We subcutaneously injected BPH1 cells alone or BPH1 cells admixed with pCAFs into nude mice fed either control or p38i chow as described for the experiments in Fig 4F. As expected, there was no difference in BPH1 cell growth whether mice were fed control or p38i chow (Fig. 5C). Importantly, in mice receiving control chow, BPH1 cells admixed with pCAFs grew significantly more than BPH1 cells injected alone, verifying that our patient-derived fibroblasts were *bona fide* CAFs (Fig. 5C). pCAF-mediated BPH1 growth was significantly inhibited in mice receiving p38i (Fig. 5C), similar to what was observed with senescent fibroblast-mediated BPH1 growth (Fig 4G and H). These findings, combined with those from p38MAPK inhibition of senescent-fibroblast driven tumors, suggest that p38MAPK is a viable, stromal specific therapeutic target that may show efficacy in diverse tumor microenvironments and diverse tumor types

DISCUSSION

The regulation of SASP expression is complex, involving the DNA damage response (16), HDAC1 activity (15), and transcriptional regulation by NFκB and C/EBPβ (17) (18) (19). p38MAPK perhaps best exemplifies the complexity of SASP regulation. Previous reports have shown that p38MAPK impacts NFκB-driven transcriptional control of SASP expression immediately following exposure to a senescence-inducing signal (19). In our system, p38MAPK inhibition had no effect on NFκB transcriptional activity when it was initiated after cells acquired the senescent phenotype as evidenced by SA-β-gal staining. However, p38MAPK inhibition did have a significant impact on SASP factor mRNA

stability. Our data are consistent with p38MAPK playing a dual role in SASP factor expression. We hypothesize that SASP factor expression is achieved through early rounds of transcription followed by post-transcriptional mRNA stabilization, both of which require distinct p38MAPK functions.

Inhibiting the SASP represents a novel stromal-specific therapeutic cancer modality that could be beneficial at multiple stages of tumorigenesis. We have demonstrated that senescent cells are present in the microenvironment before the formation of preneoplastic lesions and that SASP factors promote preneoplastic cell growth (23) (15). The SASP also promotes more aggressive malignancies by increasing angiogenesis and invasion (9) (39). Finally, the SASP is hypothesized to promote later events in cancer progression including metastasis and recurrence through its promotion of cancer stem cell formation and chemo-resistant niches (40) (41) (7). Together, these findings suggest that inhibition of the SASP will prevent the development and/or progression of malignancies. p38MAPK could provide an ideal target as it impacts both the transcriptional and post-transcriptional regulation of SASP (19) and may be particularly effective because it can inhibit SASP expression after the stabilization of SASP mRNAs has already occurred.

Our findings that oral administration of a p38MAPK inhibitor dramatically inhibits SASP-mediated tumor growth driven by senescent fibroblasts and CAFs indicate for the first time that the tumor-promoting capabilities of senescent and cancer-associated fibroblasts are mediated through similar signaling pathways. Furthermore, these findings suggest that p38MAPK is an important therapeutic target with wide applicability in a variety of tumor-promoting microenvironments. This is strengthened by our *in silico* analysis of the stromal compartment of breast cancer lesions, which we show express many p38MAPK-dependent genes. These data are intriguing in light of the fact that p38MAPK inhibitors have moved into phase II and III clinical trials for inflammatory diseases including rheumatoid arthritis, Crohn's disease, and psoriasis, demonstrating their tolerability in patients (36) (37). Given our findings, we suggest that p38MAPK inhibitors warrant investigation for use as anti-neoplastic therapy.

METHODS

Cell lines and treatments

BJ human foreskin fibroblasts were obtained from Dr. Robert Weinberg (Massachusetts Institute of Technology, Cambridge, MA) and were cultured as previously described (23). IMR90 human lung fibroblasts were purchased from ATCC (Manassas, VA) and were cultured in Dulbecco's Modified Eagle's Medium (DMEM) supplemented with 10% FBS (Sigma, St. Louis, MO) and 1% penicillin/streptomycin. Patient-derived breast cancer-associated fibroblasts were purchased from Asterand (Detroit, MI) and cultured in DMEM supplemented with 10% FBS, 1 μg/mL hydrocortisone, 5 μg/mL transferrin, 5 μg/mL insulin, and 1% penicillin/streptomycin. Fibroblasts were treated with bleomycin sulfate (100 μg/mL, Sigma, St. Louis, MO) for 24 hours, followed by incubation in normal culture medium for the time points indicated. Fibroblasts were treated with actinomycin D (10 μg/mL, Sigma, St. Louis, MO) for 24 hours, SB203580 (10 μM, Millipore, Billerica, MA) for 48 hours, or CDD-111 (also referred to as SP-006, 1 μM, Confluence Life Sciences, St.

Louis, MO) for 48 hours unless indicated otherwise. SB203580 and CDD-111 were replenished daily. Fibroblasts were treated with 2 fresh changes of 4 mM sodium butyrate (NaB, Sigma, St. Louis, MO) for 72 or 120 hours. RNA was isolated using TRI Reagent (Life Technologies, Carlsbad, CA) at the time points indicated. HaCaT preneoplastic keratinocyte cells (obtained from Dr. Norbert E. Fusenig, German Cancer Research Center, Heidelberg, Germany) stably expressing click beetle red (CBR) luciferase (HaCat-CBR) (16) were grown in DMEM supplemented with 10% heat-inactivated FBS and 1% penicillin/streptomycin (Sigma, St. Louis, MO). BPH1 preneoplastic prostate epithelial cells (obtained from Dr. Robert Weinberg, Massachusetts Institute of Technology, Cambridge, MA) stably expressing CBR luciferase (BPH1-CBR) were grown in DMEM supplemented with 10% non-heat inactivated FBS and 1% penicillin/streptomycin. All cells were cultured at 37 °C in 5% carbon dioxide and 5% oxygen. No cell lines used were authenticated.

Plasmids

The luciferase reporter construct fused to the 3' UTR of IL6 (lucIL6) was a gift from Dr. Nicholas Davidson (Washington University School of Medicine, St. Louis, MO) and was subcloned into the *Eco*RI site of pBABE-hygro. Luciferase reporter constructs fused to the 3' UTR of GMCSF or GAPDH were purchased from Switch Gear Genomics (Menlo Park, CA) and were subcloned in to pBABE-hygro using the *Sna*bI and *Sal*I restriction sites. Short hairpin RNA sequences targeting human AUF1 (shAUF1A: 5'-AGAGTGGTTATGGGAAGGTAT-3', shAUF1B: 5'-AGTAAGAACGAGGAGGATGAA-3'), p38 (5'-GCCGTATAGGATGTCAGACAA-3') and Hsp27 (5-CCCGGACGAGCTGACGGTCAA-3') were obtained from the Children's Discovery Institute's viral vector-based RNAi core at Washington University in St. Louis, and were supplied in the pLKO.1-puro backbone. Luciferase reporter assays were performed using a plasmid containing an NFκB-responsive promoter driving expression of firefly luciferase (NFκB-luc) and a plasmid encoding *Renilla* luciferase driven by the thymidine kinase promoter, obtained from Dr. David Piwnica-Worms (Washington University School of Medicine, St. Louis, MO).

Senescence-associated β-galactosidase (SA-β-gal) staining

SA-β-gal staining was carried out as described previously (23).

Quantitative PCR

cDNA synthesis and quantitative PCR was performed using previously published protocols and manufacturers' instructions (42) (SYBR Green, Life Technologies, Carlsbad, CA). Primers for GAPDH (F: 5'-GCATGGCCTTCGGTGTCC-3', R: 5'-AATGCCAGCCCCAGCGTCAAA-3'), IL6 (F: 5'-ACATCCTCGACGGCATCTCA-3', R: 5'-TCACCAGGCAAGTCTCCTCA-3'), IL8 (F: 5'-GCTCTGTGTGAAGGTGCAGT-3', R: 5'-TGCACCCAGTTTTCCTTGGG-3'), MMP3 (F: 5'-GTTTTGGCCCATGCCTATGCCCC-3', R: 5'-GGAGTCAGGGGGAGGTCCATAGAGG-3'), CCL20 (F: 5'-CTGCGGCGAATCAGAAGCAGC-3', R: 5'-CCTTCATTGGCCAGCTGCCGT-3'), lucIL6 (F: 5'-CGGGCGCGGTCGGTAAAGTT-3', R: 5'-

AAACAACAACGGCGGCGGGA-3'), and lucGMCSF and lucGAP (F: 5'-GAGAAACATGCGGAGAACGC-3', R: 5'-AGCATGCACGATAGCCTTGA-3') were purchased from IDT. GMCSF cDNA was amplified using a Taqman probe/primer set (catalog number Hs00929873_m1, Life Technologies, Carlsbad, CA).

ELISA

Conditioned medium was generated by incubating cells for 24 hours in serum-free medium. Following collection, secreted IL6 protein levels were measured using the human IL6 Quantikine ELISA kit (catalog number D6050, R&D Systems, Minneapolis, MN).

Western blot analysis

Cell pellets were lysed in buffer containing 50 mM Tris pH 8.0, 5 mM EDTA, 0.5% NP40 and 100 mM sodium chloride for 20 minutes at 4 °C. Protein concentration was quantified using the Bradford Protein Assay (Bio-Rad, Berkeley, CA). The primary antibodies used were: polyclonal AUF1 (Millipore, Billerica, MA, catalog number 07260MI) at 1:3000, polyclonal p-p38 (PhosphoSolutions, Aurora, CO, catalog number p190-1802) at 1:1000, polyclonal p38 (Cell Signaling, Boston, MA, catalog number 9218) at 1:1000, monoclonal β-catenin (BD Biosciences, San Jose, CA, catalog number 610153) at 1:5000, and monoclonal α-tubulin (Abcam, Cambridge, MA, product number ab6160) at 1:1000. All secondary antibodies from the appropriate species were horseradish peroxidase-conjugated (Jackson Laboratories, Bar Harbor, ME) and diluted 1:10000.

Virus Production

Virus was produced as described previously (23).

RNA-binding protein immunoprecipitation (RIP)

Cell pellets from 7×10^7 BJ fibroblasts were lysed in the same buffer used for western blot analysis. Protein concentration was analyzed using the Bradford Protein Assay (Bio-Rad, Berkeley, CA). 3 mg of protein was used for each immunoprecipitation. The following primary antibody was used: 30 μg of polyclonal AUF1 (Millipore, Billerica, MA, catalog number 07260MI). Equivalent amounts of normal IgG antibody (Cell Signaling, Boston, MA) were used to control for specific immunoprecipitation. Cell lysates were pre-cleared with 20 μL protein A Dynabeads (Life Technologies, Carlsbad, CA) for 30 minutes at 4 °C prior to immunoprecipitation. 100 μL Protein A Dynabeads were used for each immunoprecipitation. Beads were washed 3 times in 0.1 M monosodium phosphate and then incubated in 0.1 M monosodium phosphate with the appropriate antibody for at least 1 hour at room temperature. Beads were then washed 3 times in Buffer A (1× PBS, 0.1% SDS, 0.3% sodium deoxycholate, 0.3% NP40), followed by incubation for 30 minutes at room temperature in NT2 buffer (50 mM Tris pH 7.4, 150 mM sodium chloride, 1 mM magnesium chloride). Antibody-bound beads were then added to pre-cleared cell lysates, and immunoprecipitated overnight at 4 °C. 100 μL of cell lysate was removed from the IgG immunoprecipitation to be used for input controls. Immunoprecipitated beads were washed 2 times with each of the following buffers: Buffer A, Buffer B (5× PBS, 0.1% SDS, 0.5% sodium deoxycholate, 0.5% NP40) and Buffer C (50 mM Tris pH 7.4, 10 mM magnesium

chloride, 0.5% NP40). Beads were then resuspended in NT2 containing 0.1% SDS, 80 U RNase OUT (Life Technologies, Carlsbad, CA), and 30 μg Proteinase K and incubated at 55 °C for 30 minutes. RNA was isolated from the beads by adding 1 mL of TRI Reagent (Life Technologies, Carlsbad, CA). Following cDNA synthesis, mRNA levels of SASP factors were analyzed by qPCR using the primers and procedures described above.

Luciferase reporter assay

BJ fibroblasts were transiently transfected with plasmids encoding NFκB-luc and *Renilla* luciferase. *Renilla* luciferase expression was used to standardize for transfection efficiency. Transfection was performed using manufacturer's protocol for the Lipofectamine 2000 reagent (Life Technologies, Carlsbad, CA). Luciferase activities were measured 48 hours post-transfection using live cell imaging as described (43).

Co-culture

Co-culture experiments were performed as previously described with the following modifications (23). 1.3×10^4 fibroblasts were plated in black-walled 96 well plates (Fisher Scientific, Pittsburgh, PA). Cells were incubated in starve medium (DMEM + 1% penicllin/ streptomycin) for 3 days before the addition of HaCat-CBR cells. SB203580 was refreshed daily until HaCaT-CBR plating. HaCat-CBR cells were cultured in starve medium for 24 hours prior to plating on fibroblasts. 1.0×10^3 HaCat-CBR cells were plated on fibroblasts and incubated for the indicated length of time. At the times indicated, D-luciferin (Biosynth, Naperville, IL) was added to a final concentration of 150 μg/mL. After ten minutes, plates were imaged using an IVIS 100 camera (PerkinElmer, Downers Grove, IL) using the following settings: exposure=10 s–5 min, field of view=15, binning=16, f/stop=1, open filter.

Xenografts

1×10^6 BPH1-CBR preneoplastic prostate epithelial cells were co-injected with 1×10^6 BJ human foreskin fibroblasts. Cells were injected subcutaneously in a 50:50 mixture of DMEM:growth factor-reduced Matrigel (BD Biosciences, San Jose, CA) into the rear flanks of female NcR nude mice (Taconic, Germantown, NY). In vivo bioluminescence imaging was performed on the days indicated on an IVIS 100 (PerkinElmer, Downers Grove, IL; Living Image 3.2, 1–60 s exposures, binning 4, 8 or, 16, FOV 15 cm, f/stop 1, open filter) following IP injection of D-luciferin (150 mg/kg; Biosynth, Naperville, IL). For analysis, total photon flux (photons/sec) was measured from a fixed region of interest over the xenografts using Living Image 2.6 (PerkinElmer, Downers Grove, IL).

RNA Sequence Analysis

Total RNA was isolated using TRI Reagent (Life Technologies, Carlsbad, CA) and the RiboPure RNA isolation kit (Life Technologies, Carlsbad, CA) following the manufacturer's instructions. Ribosomal RNA was removed by poly-A selection using oligo-dT beads. mRNA was then fragmented and reverse transcribed to yield double stranded cDNA using random hexamers. cDNA was blunt ended, had an A base added to the 3' ends, and then had Illumina sequencing adapters ligated to the ends. Ligated fragments were then

amplified for 12 cycles using primers incorporating unique index tags. Fragments were sequenced on an Illumina HiSeq-2000 (San Diego, CA) using single reads extending 50 bases. Raw data was de-multiplexed and aligned to the reference genome using TopHat. Transcript abundances were then estimated from the alignment files using Cufflinks. EdgeR was used for differential expression analysis.

Generation of CAFs

Primary breast tissue was collected without patient identifiers in compliance with a protocol approved by the Brigham and Women's Hospital (Institutional Review Board 93-085). Fibroblasts were isolated (10) (11) and immortalized through expression of hTERT-GFP (44) as previously described.

To generate cancer-associated fibroblasts (CAFs), 3×10^6 human mammary fibroblasts were co-injected with 1×10^6 MCF7-Ras tumor cells subcutaneously into nude mice. After tumors reached 1 cm, mice were euthanized and CAFs were re-isolated by digesting tissues in 1 mg/ml collagenase A for 1–4 hours at 37 °C with continuous rotation. Resulting cell suspensions were dispersed with an 18-gauge needle, washed 2 times with resuspension buffer (2% heat-inactivated fetal calf serum in sterile Hank's Balanced Salt Solution (HBSS)), and filtered through 70 μm nylon mesh. GFP+ CAFs were then isolated by fluorescence-activated cell sorting and maintained under their standard culture conditions. CAFs were confirmed to be human by staining with human specific mitochondrial DNA (data not shown).

Oral dosage of p38MAPK inhibitor

The p38MAPK small molecule inhibitor CDD-111 (Confluence Life Sciences, Inc, St. Louis, MO) was compounded at 516 ppm with Purina Rodent Chow #5001 (St. Louis, MO) to generate a daily exposure of 80 mg/kg/day. Female NcR nude mice (Taconic, Germantown, NY) were fed ad libitum.

LPS challenge and TNFα ELISA

Female NcR nude mice (Taconic, Germantown, NY) were fed ad libitum for 3 days. 100 ng lipopolysaccharide (LPS) (Sigma, St. Louis, MO) was then administered by IP injection. Serum was collected 1 hour after LPS dosage. TNFα levels were analyzed by ELISA (R&D Systems, Minneapolis, MN)

Staining of xenograft tumors

Following excision, tumors were fixed in 10% formalin and embedded in paraffin for sectioning. Standard H&E technique was used for all sections. Serial sections were stained for Ki67 (1:50, catalog number 550609, BD Bioscience, San Jose, CA), p16 (1:100, catalog number sc-1661, Santa Cruz Biotechnology, Dallas, TX) and vimentin (1:700, catalog number ab45939, Abcam, Cambridge, MA).

Statistical Analysis

Data is presented as the mean ± SEM. Statistical significance was determined using the Student's *t* test, with a p value < 0.05 considered significant. Percent mRNA remaining was calculated as the fold mRNA in ActD-treated SIPS cells over untreated SIPS cells. Overrepresented gene ontology terms in the expression data were identified using a Fisher's exact test, with a significance threshold of $p < 0.05$ as implemented in GOstat (45).

Supplementary Material

Refer to Web version on PubMed Central for supplementary material.

Acknowledgments

We thank Dr. Nicholas Davidson for the lucIL6 construct and advice on the RIP protocol. We thank Julie Prior and The BRIGHT Institute at Washington University School of Medicine for live animal imaging and advice and Amey Barakat for technical assistance with mitochondrial DNA staining. RNAi constructs for this project were obtained through the Board Instituted and funded in part by the Children's Discovery Institute of Washington University and St. Louis. We thank the Genome Technology Access Center in the Department of Genetics at Washington University School of Medicine for help with genomic analysis. The Center is supported by NCI Cancer Center Support Grant P30 CA91842 to the Siteman Cancer Center and by ICTS/CTSA Grant UL1RR024992 from the National Center for Research Resources (NCRR). We thank Dr. John Edwards for assistance in RNA-seq analyses. We thank Mr. Daniel Teasley, Dr. Michelle Hurchla, Dr. Katherine Weilbaecher, Dr. Gregory Longmore, Dr. Andrey Shaw and Dr. Kendall Blumer for critical reading of the manuscript. We thank Dr. Craig Allred for advice on human expression. We thank Mr. Adnan Elhammali for assistance with GO processes analysis.

Financial Support: NIH 5 R01 CA130919 (SAS), NIH Cellular Biochemical and Molecular Sciences Pre-doctoral Training Grant T32 GM007067 (EA and KCF), American Cancer Society Research Scholar Award (SAS and SSM), NIH RO1 CA166284-01 (SSM). Molecular imaging was funded by NIH P50 CA94056 (DPW). Histological analysis was supported by NIH P30 AR057235 to the Washington University Musculoskeletal Research Center (DVN). The RNAi constructs were obtained from the Viral-vector-based RNAi Core at Washington University, which is support by a grant from the Children's Discovery Institute and Broad Institute.

Abbreviations

SASP	Senescence associated secretory phenotype
SIPS	stress-induced premature senescence
CAFs	cancer associated fibroblasts
TME	tumor microenvironment
p38MAPK	mitogen-activated protein kinase p38
LCM	laser capture micro-dissection
ActD	actinomycin D
RS	replicative senescence
NaB	sodium butyrate
UTR	untranslated region
sh	short hairpin
RIP	RNA-binding protein immunoprecipitation

BC	breast cancer
CBR	click-beetle red luciferase
NMF	normal mammary fibroblast
TNFα	tumor necrosis factor α
NFκB	nuclear factor κB
SA-β-gal	senescence-associated β-galactosidase
LPS	lipopolysaccharide

REFERENCES

1. Finak G, Bertos N, Pepin F, Sadekova S, Souleimanova M, Zhao H, et al. Stromal gene expression predicts clinical outcome in breast cancer. Nat Med. 2008; 14:518–527. [PubMed: 18438415]
2. Ma XJ, Dahiya S, Richardson E, Erlander M, Sgroi DC. Gene expression profiling of the tumor microenvironment during breast cancer progression. Breast Cancer Res. 2009; 11:R7. [PubMed: 19187537]
3. Karnoub AE, Dash AB, Vo AP, Sullivan A, Brooks MW, Bell GW, et al. Mesenchymal stem cells within tumour stroma promote breast cancer metastasis. Nature. 2007; 449:557–563. [PubMed: 17914389]
4. Olumi AF, Grossfeld GD, Hayward SW, Carroll PR, Tlsty TD, Cunha GR. Carcinoma-associated fibroblasts direct tumor progression of initiated human prostatic epithelium. Cancer research. 1999; 59:5002–5011. [PubMed: 10519415]
5. Dimri GP, Lee X, Basile G, Acosta M, Scott G, Roskelley C, et al. A biomarker that identifies senescent human cells in culture and in aging skin in vivo. Proceedings of the National Academy of Sciences of the United States of America. 1995; 92:9363–9367. [PubMed: 7568133]
6. Bavik C, Coleman I, Dean JP, Knudsen B, Plymate S, Nelson PS. The gene expression program of prostate fibroblast senescence modulates neoplastic epithelial cell proliferation through paracrine mechanisms. Cancer research. 2006; 66:794–802. [PubMed: 16424011]
7. Parrinello S, Coppe JP, Krtolica A, Campisi J. Stromal-epithelial interactions in aging and cancer: senescent fibroblasts alter epithelial cell differentiation. Journal of cell science. 2005; 118:485–496. [PubMed: 15657080]
8. Krtolica A, Parrinello S, Lockett S, Desprez PY, Campisi J. Senescent fibroblasts promote epithelial cell growth and tumorigenesis: a link between cancer and aging. Proceedings of the National Academy of Sciences of the United States of America. 2001; 98:12072–12077. [PubMed: 11593017]
9. Coppe JP, Patil CK, Rodier F, Sun Y, Munoz DP, Goldstein J, et al. Senescence-associated secretory phenotypes reveal cell-nonautonomous functions of oncogenic RAS and the p53 tumor suppressor. PLoS biology. 2008; 6:2853–2868. [PubMed: 19053174]
10. Elkabets M, Gifford AM, Scheel C, Nilsson B, Reinhardt F, Bray MA, et al. Human tumors instigate granulin-expressing hematopoietic cells that promote malignancy by activating stromal fibroblasts in mice. The Journal of clinical investigation. 2011; 121:784–799. [PubMed: 21266779]
11. Orimo A, Gupta PB, Sgroi DC, Arenzana-Seisdedos F, Delaunay T, Naeem R, et al. Stromal fibroblasts present in invasive human breast carcinomas promote tumor growth and angiogenesis through elevated SDF-1/CXCL12 secretion. Cell. 2005; 121:335–348. [PubMed: 15882617]
12. Erez N, Truitt M, Olson P, Arron ST, Hanahan D. Cancer-Associated Fibroblasts Are Activated in Incipient Neoplasia to Orchestrate Tumor-Promoting Inflammation in an NF-kappaB-Dependent Manner. Cancer cell. 2010; 17:135–147. [PubMed: 20138012]
13. Hu M, Polyak K. Microenvironmental regulation of cancer development. Current opinion in genetics & development. 2008; 18:27–34. [PubMed: 18282701]

14. Allinen M, Beroukhim R, Cai L, Brennan C, Lahti-Domenici J, Huang H, et al. Molecular characterization of the tumor microenvironment in breast cancer. Cancer cell. 2004; 6:17–32. [PubMed: 15261139]
15. Pazolli E, Alspach E, Milczarek A, Prior J, Piwnica-Worms D, Stewart SA. Chromatin remodeling underlies the senescence-associated secretory phenotype of tumor stromal fibroblasts that supports cancer progression. Cancer research. 2012; 72:2251–2261. [PubMed: 22422937]
16. Rodier F, Coppe JP, Patil CK, Hoeijmakers WA, Munoz DP, Raza SR, et al. Persistent DNA damage signalling triggers senescence-associated inflammatory cytokine secretion. Nature cell biology. 2009; 11:973–379.
17. Kuilman T, Michaloglou C, Vredeveld LC, Douma S, van Doorn R, Desmet CJ, et al. Oncogene-induced senescence relayed by an interleukin-dependent inflammatory network. Cell. 2008; 133:1019–1031. [PubMed: 18555778]
18. Chien Y, Scuoppo C, Wang X, Fang X, Balgley B, Bolden JE, et al. Control of the senescence-associated secretory phenotype by NF-kappaB promotes senescence and enhances chemosensitivity. Genes & development. 2011; 25:2125–2136. [PubMed: 21979375]
19. Freund A, Patil CK, Campisi J. p38MAPK is a novel DNA damage response-independent regulator of the senescence-associated secretory phenotype. Embo J. 2011; 30:1536–1548. [PubMed: 21399611]
20. Winzen R, Kracht M, Ritter B, Wilhelm A, Chen CY, Shyu AB, et al. The p38 MAP kinase pathway signals for cytokine-induced mRNA stabilization via MAP kinase-activated protein kinase 2 and an AU-rich region-targeted mechanism. The EMBO journal. 1999; 18:4969–4980. [PubMed: 10487749]
21. Zhao W, Liu M, Kirkwood KL. p38alpha stabilizes interleukin-6 mRNA via multiple AU-rich elements. The Journal of biological chemistry. 2008; 283:1778–1785. [PubMed: 18042545]
22. Knapinska AM, Gratacos FM, Krause CD, Hernandez K, Jensen AG, Bradley JJ, et al. Chaperone Hsp27 modulates AUF1 proteolysis and AU-rich element-mediated mRNA degradation. Molecular and cellular biology. 2011; 31:1419–1431. [PubMed: 21245386]
23. Pazolli E, Luo X, Brehm S, Carbery K, Chung JJ, Prior JL, et al. Senescent Stromal-Derived Osteopontin Promotes Preneoplastic Cell Growth. Cancer research. 2009
24. Liu D, Hornsby PJ. Senescent human fibroblasts increase the early growth of xenograft tumors via matrix metalloproteinase secretion. Cancer research. 2007; 67:3117–3126. [PubMed: 17409418]
25. Freund A, Patil CK, Campisi J. p38MAPK is a novel DNA damage response-independent regulator of the senescence-associated secretory phenotype. The EMBO journal. 2011; 30:1536–1548. [PubMed: 21399611]
26. Cuenda A, Rouse J, Doza YN, Meier R, Cohen P, Gallagher TF, et al. SB 203580 is a specific inhibitor of a MAP kinase homologue which is stimulated by cellular stresses and interleukin-1. FEBS letters. 1995; 364:229–233. [PubMed: 7750577]
27. Guhaniyogi J, Brewer G. Regulation of mRNA stability in mammalian cells. Gene. 2001; 265:11–23. [PubMed: 11255003]
28. Paschoud S, Dogar AM, Kuntz C, Grisoni-Neupert B, Richman L, Kuhn LC. Destabilization of interleukin-6 mRNA requires a putative RNA stem-loop structure, an AU-rich element, and the RNA-binding protein AUF1. Molecular and cellular biology. 2006; 26:8228–8241. [PubMed: 16954375]
29. Raineri I, Wegmueller D, Gross B, Certa U, Moroni C. Roles of AUF1 isoforms, HuR and BRF1 in ARE-dependent mRNA turnover studied by RNA interference. Nucleic acids research. 2004; 32:1279–1288. [PubMed: 14976220]
30. Sarkar S, Han J, Sinsimer KS, Liao B, Foster RL, Brewer G, et al. RNA-binding protein AUF1 regulates lipopolysaccharide-induced IL10 expression by activating IkappaB kinase complex in monocytes. Molecular and cellular biology. 2011; 31:602–615. [PubMed: 21135123]
31. Strieter RM, Burdick MD, Gomperts BN, Belperio JA, Keane MP. CXC chemokines in angiogenesis. Cytokine & growth factor reviews. 2005; 16:593–609. [PubMed: 16046180]
32. Liu J, Zhang N, Li Q, Zhang W, Ke F, Leng Q, et al. Tumor-associated macrophages recruit CCR6+ regulatory T cells and promote the development of colorectal cancer via enhancing CCL20 production in mice. PloS one. 2011; 6:e19495. [PubMed: 21559338]

33. Ernst M, Najdovska M, Grail D, Lundgren-May T, Buchert M, Tye H, et al. STAT3 and STAT1 mediate IL-11-dependent and inflammation-associated gastric tumorigenesis in gp130 receptor mutant mice. The Journal of clinical investigation. 2008; 118:1727–1738. [PubMed: 18431520]
34. Apte RN, Dotan S, Elkabets M, White MR, Reich E, Carmi Y, et al. The involvement of IL-1 in tumorigenesis, tumor invasiveness, metastasis and tumor-host interactions. Cancer metastasis reviews. 2006; 25:387–408. [PubMed: 17043764]
35. Uhlirova M, Bohmann D. JNK- and Fos-regulated Mmp1 expression cooperates with Ras to induce invasive tumors in Drosophila. The EMBO journal. 2006; 25:5294–5304. [PubMed: 17082773]
36. Cohen P. Protein kinases--the major drug targets of the twenty-first century? Nature reviews Drug discovery. 2002; 1:309–315.
37. Saklatvala J. The p38 MAP kinase pathway as a therapeutic target in inflammatory disease. Current opinion in pharmacology. 2004; 4:372–377. [PubMed: 15251131]
38. Burnette BL, Selness S, Devraj R, Jungbluth G, Kurumbail R, Stillwell L, et al. SD0006: a potent, selective and orally available inhibitor of p38 kinase. Pharmacology. 2009; 84:42–60. [PubMed: 19590255]
39. Coppe JP, Kauser K, Campisi J, Beausejour CM. Secretion of vascular endothelial growth factor by primary human fibroblasts at senescence. The Journal of biological chemistry. 2006; 281:29568–29574. [PubMed: 16880208]
40. Gilbert LA, Hemann MT. DNA damage-mediated induction of a chemoresistant niche. Cell. 2010; 143:355–366. [PubMed: 21029859]
41. Cahu J, Bustany S, Sola B. Senescence-associated secretory phenotype favors the emergence of cancer stem-like cells. Cell death & disease. 2012; 3:e446. [PubMed: 23254289]
42. Coppe JP, Boysen M, Sun CH, Wong BJ, Kang MK, Park NH, et al. A role for fibroblasts in mediating the effects of tobacco-induced epithelial cell growth and invasion. Molecular cancer research : MCR. 2008; 6:1085–1098. [PubMed: 18644973]
43. Moss BL, Gross S, Gammon ST, Vinjamoori A, Piwnica-Worms D. Identification of a ligand-induced transient refractory period in nuclear factor-kappaB signaling. The Journal of biological chemistry. 2008; 283:8687–8698. [PubMed: 18203717]
44. Hahn WC, Counter CM, Lundberg AS, Beijersbergen RL, Brooks MW, Weinberg RA. Creation of human tumour cells with defined genetic elements. Nature. 1999; 400:464–468. [PubMed: 10440377]
45. Beissbarth T, Speed TP. GOstat: find statistically overrepresented Gene Ontologies within a group of genes. Bioinformatics. 2004; 20:1464–1465. [PubMed: 14962934]

SIGNIFICANCE

The TME plays a key role in tumorigenesis. We demonstrate that p38MAPK governs a post-transcriptional mechanism that sustains the protumorigenic SASP. Inhibition of p38MAPK abrogates the tumor promoting activities of CAFs and senescent fibroblasts. Thus, p38MAPK is a TME-specific Achilles' heel that may be exploited as a new therapeutic target.

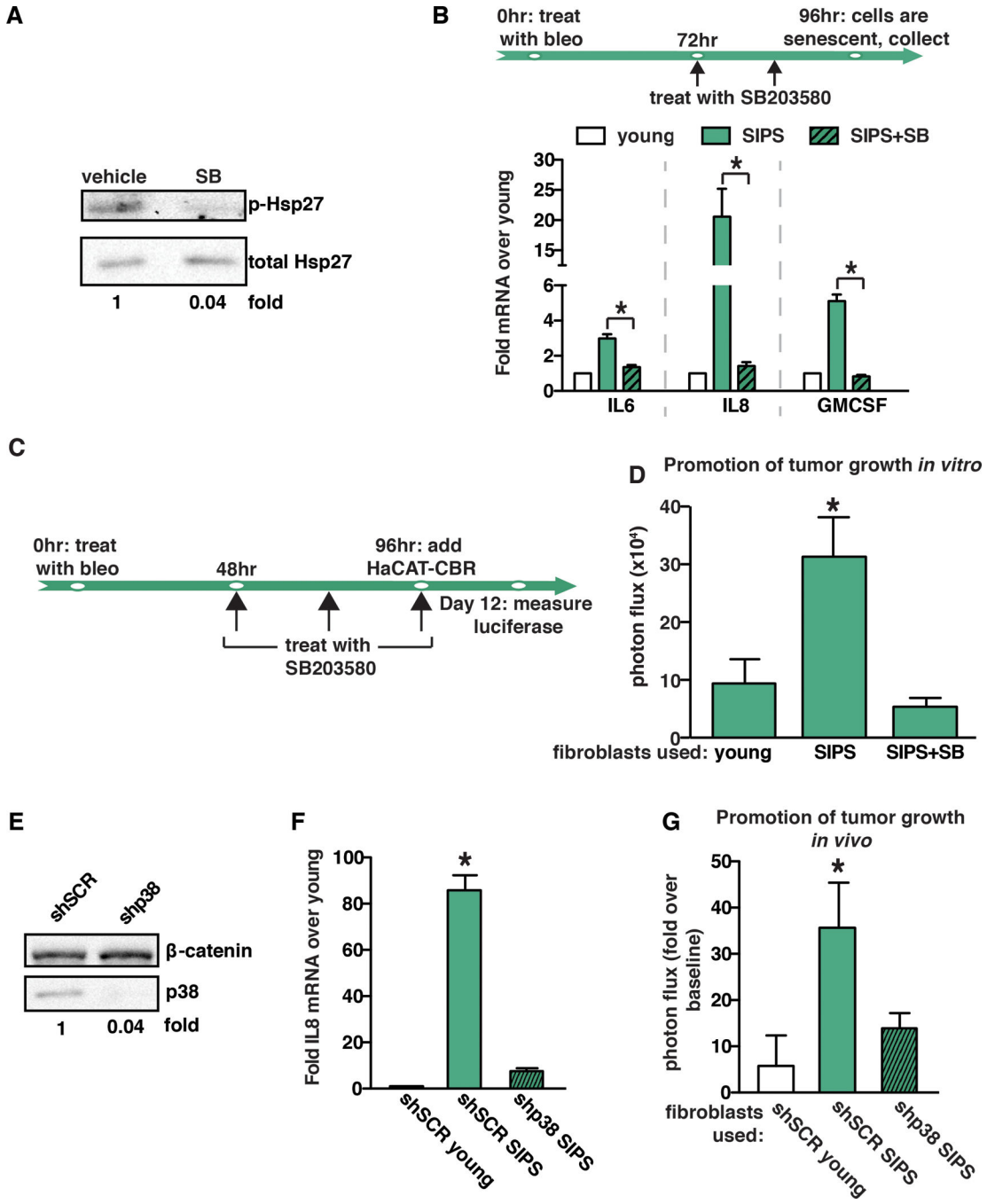

Fig. 1. p38MAPK activity controls the pro-tumorigenic properties of the SASP

(**A**) Western blot analysis demonstrating that SB203580 treatment inhibits p38MAPK activity. As expected, SB203580 treatment significantly impacts phosphorylation of p38MAPK's direct downstream target, Hsp27. Total Hsp27 was used as loading control. (**B**) Schematic of protocol to generate SIPS in BJ fibroblasts. Cells were treated with bleomycin for 24 hours. SB203580 (SB) treatment or vehicle control was initiated 48 hours after removal of bleomycin (bleo). 96 hours after bleomycin treatment, cells were collected

for expression analysis of IL6, IL8, and GMCSF by qRT-PCR. SIPS: senescence induced premature senescence. Representative experiment, n=4.

(**C**) Timeline of bleomycin (bleo) and SB203580 treatment of BJ fibroblasts in (d). SB203580 was replenished daily until co-culture with HaCAT-CBR cells was initiated.

(**D**) Growth of human keratinocytes expressing click beetle red (HaCaT-CBR) measured 8 days following initiation of co-culture with indicated fibroblast populations. Representative experiment, n=3.

(**E**) BJ fibroblasts were depleted of p38MAPK through the expression of shRNA (shp38) or control shRNA (shSCR). p38 depletion was verified by western blot analysis and β-catenin was used as a loading control.

(**F**) Expression of IL8 was analyzed by qRT-PCR 96 hours following bleomycin treatment in p38MAPK-depleted (shp38) or control (shSCR) fibroblasts and represented relative to young fibroblasts expressing shSCR control. Representative experiment, n=3.

(**G**) BJ fibroblasts expressing shp38 or shSCR were treated with bleomycin 72 hours prior to injection. Indicated fibroblast populations were admixed with preneoplastic epithelial cells expressing click beetle red (BPH1-CBR cells) and injected subcutaneously into the rear flanks of female NcR nude mice. Luciferase activity was measured using live, whole-animal imaging to monitor BPH1 cell growth relative to baseline signal. Data represents mean + SEM, n=8.

Data represents mean + SD unless otherwise stated. * indicates $p<0.05$. SIPS: stress induced premature senescence.

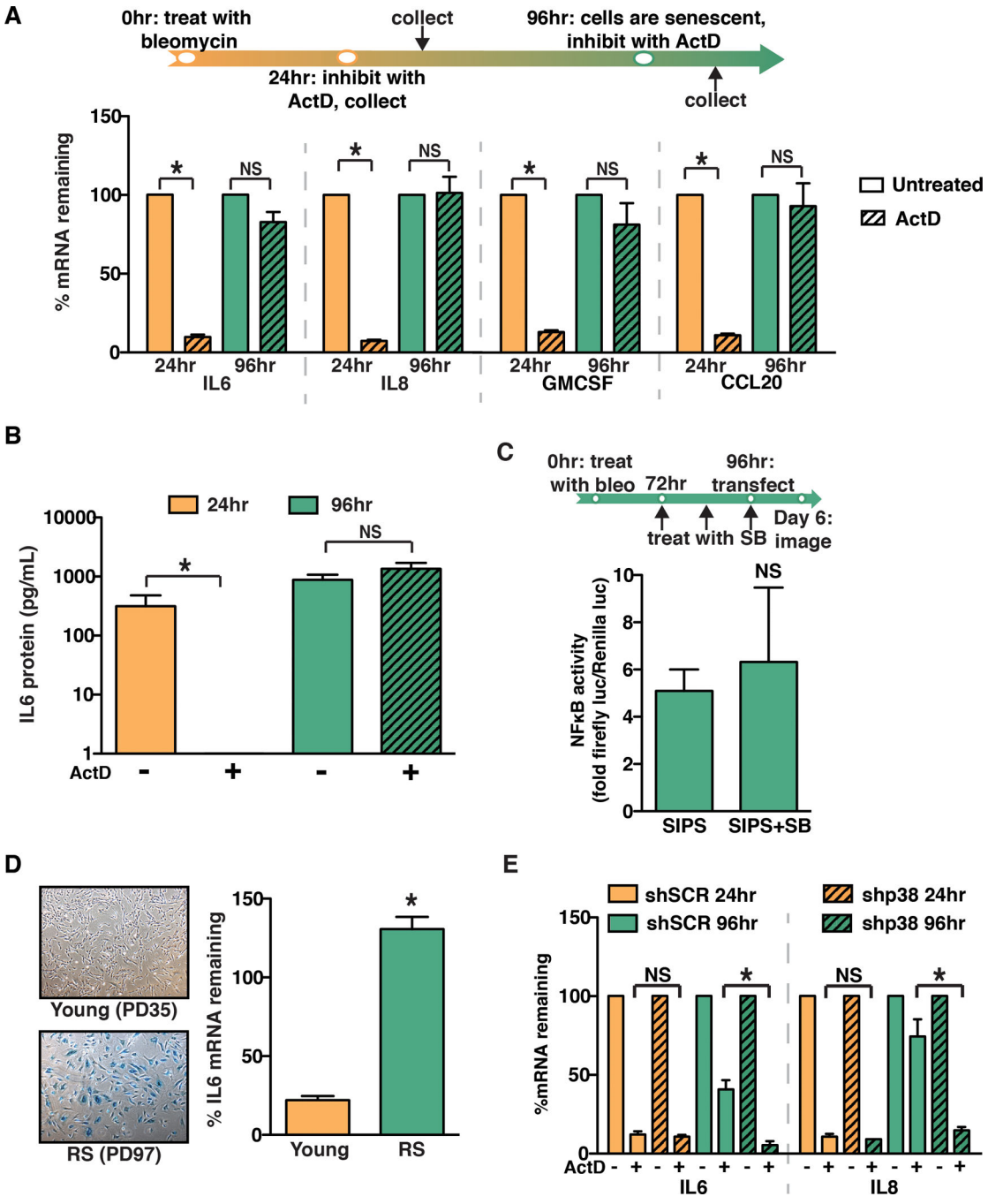

Fig. 2. p38MAPK post-transcriptionally regulates the SASP

(**A**) Schematic of protocol to generate SIPS in BJ fibroblasts. Cells were treated with bleomycin for 24 hours. Cells were subsequently treated with actinomycin D (ActD) for 24 hours. The ActD treatment was initiated 24 or 96 hours after the completion of bleomycin treatment. IL6, IL8, GMCSF, and CCL20 mRNA levels were analyzed by qRT-PCR. To account for changes in gene expression, levels mRNA in ActD-treated cells were normalized to the levels observed in untreated cells from the respective time points (% mRNA remaining). Representative experiment, n=3.

(**B**) ELISA analysis of IL6 protein levels in conditioned media from cells treated as in (**A**). Representative experiment, n=4.

(**C**) BJ fibroblasts were treated with bleomycin (bleo) for 24 hours and with SB203580 (SB) as indicated. 96 hours post bleomycin treatment cells were transiently transfected with an NFκB activity luciferase reporter. Luciferase activity was measured by live-cell imaging 48 hours post transfection. Representative experiment, n=2.

(**D**) Young BJ fibroblasts (35 population doublings, PD) or replicatively senescent BJ fibroblasts (PD97) were stained for senescence-associated β-galactosidase to confirm senescent phenotype (left). Cells were treated with ActD and IL6 mRNA levels were analyzed by qRT-PCR. Representative experiment, n=3.

(**E**) BJ fibroblasts expressing a control hairpin (shSCR) or shp38 were treated for 24 hours with ActD at 24 or 96 hours after the completion of bleomycin treatment. IL6 and IL8 mRNA levels were analyzed by qRT-PCR. Representative experiment, n=2.

Data represent mean + SD. * indicates $p<0.05$. SIPS: stress-induced premature senescence.

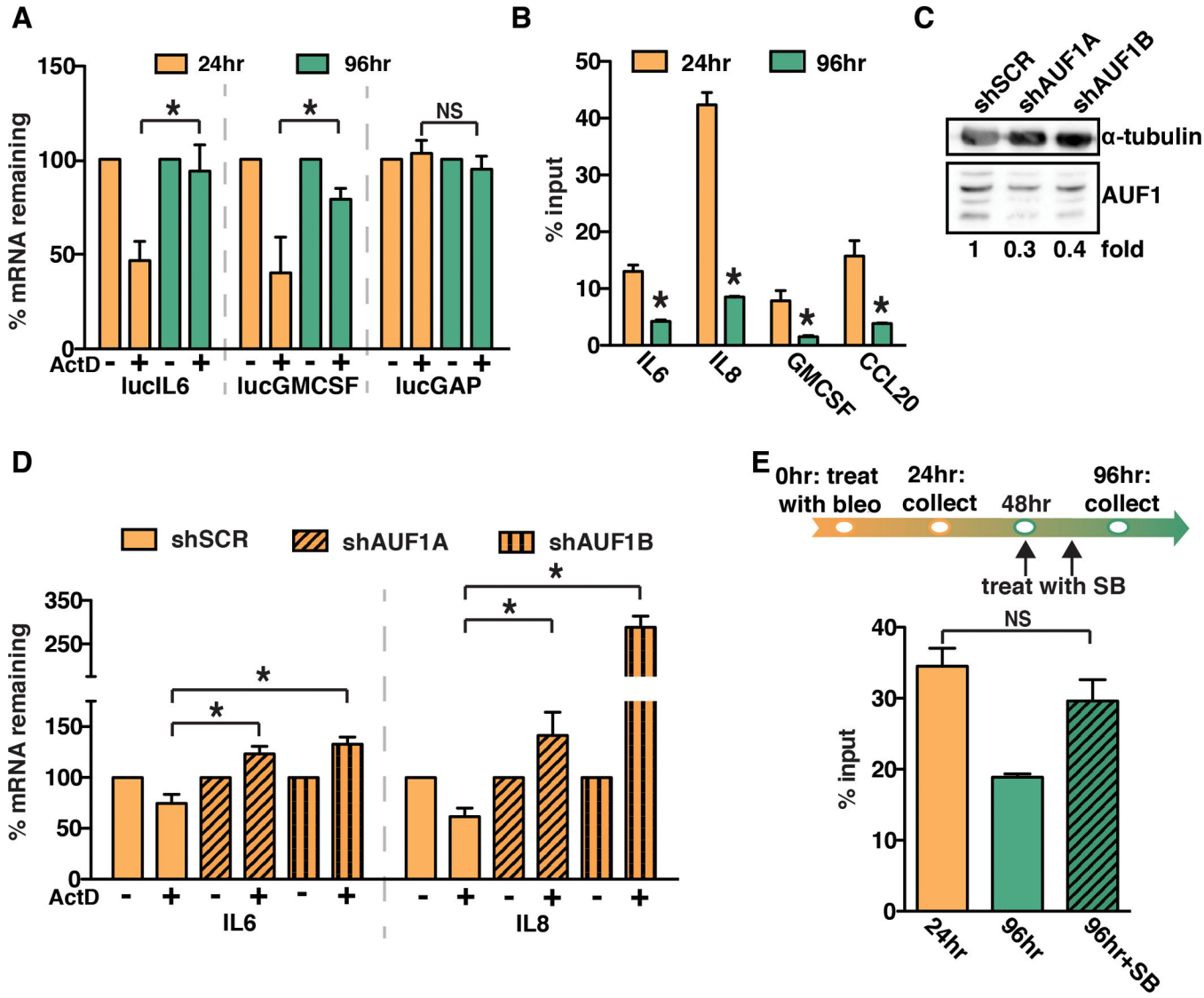

Fig. 3. AUF1 directly binds to SASP factor mRNA and modulates SASP factor stabilization

(**A**) BJ fibroblasts were stably transduced with luciferase constructs fused to the 3' untranslated regions (UTR) of IL6, GMCSF, and GAPDH (lucIL6, lucGMCSF, and lucGAP). Cells were treated with ActD at 24 or 96 hours following bleomycin treatment. Luciferase mRNA levels were analyzed by qRT-PCR. Representative experiment, n=3.

(**B**) RNA immunoprecipitation was performed for AUF1 using BJ fibroblast cell lysates collected 24 or 96 hours after bleomycin treatment. IL6, IL8, GMCSF, and CCL20 mRNA levels in immunoprecipitations were analyzed by qRT-PCR. Representative experiment, n=4.

(C) BJ fibroblasts were transduced with shRNAs to deplete AUF1 (shAUF1A and shAUF1B) or a control shRNA (shSCR). Protein levels were analyzed by western blot analysis. Note: there are four AUF1 isoforms present and α-tubulin was used as a loading control.

(**D**) 24 hours following bleomycin treatment, BJ fibroblasts expressing a control hairpin shSCR, shAUF1A, or shAUF1B were treated with ActD for 1 hour. IL6 and IL8 mRNA levels were analyzed by qRT-PCR. Representative experiment, n=2.
(**E**) RNA immunoprecipitation for AUF1 was performed on BJ fibroblasts treated with bleomycin (bleo) and SB203580 (SB) as indicated. The level of IL8 mRNA in the AUF1 immunoprecipitation was measured by qRT-PCR. Representative experiment, n=3.
Data represent mean + SD. * indicates $p<0.05$.

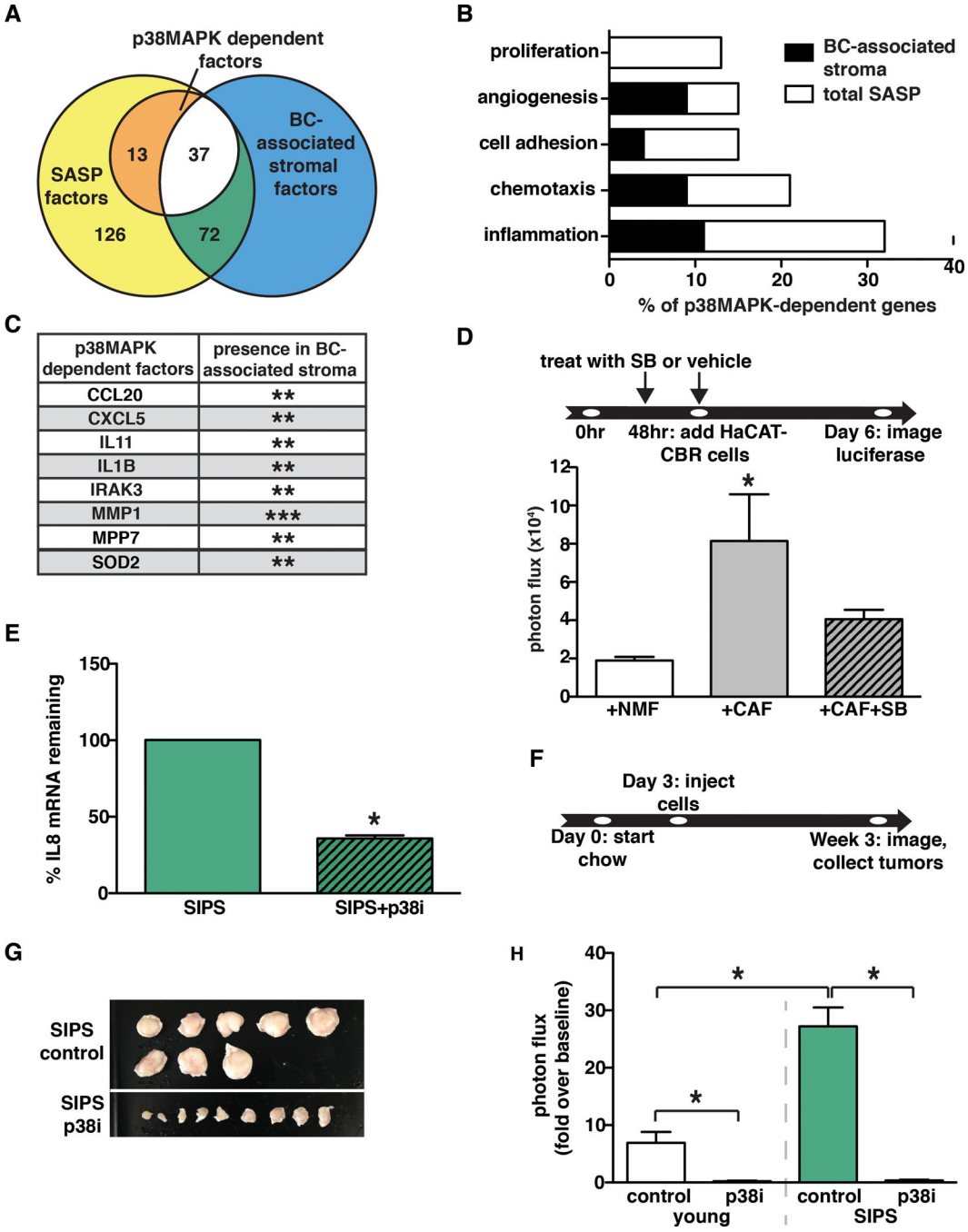

Fig. 4. p38MAPK-dependent factors are expressed in the TME of breast cancer lesions

(**A**) RNA-seq analysis was performed on young fibroblasts, senescent fibroblasts, and senescent fibroblasts treated with SB203580. RNA-seq results were analyzed to determine the number of factors upregulated in response to senescence (SASP factors) and the number of p38MAPK-dependent factors. These results were also analyzed for overlap with the expression profiles of breast cancer (BC)-associated stroma.

(**B**) GO processes analysis was performed on p38MAPK-dependent SASP factors. Results are presented as the percent of p38MAPK-depenedent genes assigned to the processes

shown. Black regions of the bars represent the percent of p38MAPK-dependent SASP factors assigned to each process that are also expressed in BC-associated stroma. The significance threshold was set at $p < 0.05$.

(**C**) p38MAPK-dependent SASP factors that are expressed in more than one BC-associated stroma data set. **indicates expression in 2 BC-associated stroma datasets, ***indicates expression in 3 BC-associated stroma datasets.

(**D**) Tumor-educated human CAFs and their normal isogenic counterparts (NMF) were treated with SB203580 (SB) or vehicle as indicated and replenished daily until co-culture with HaCAT-CBR preneoplastic keratinocytes was initiated. Luciferase activity was measured using live-cell imaging 4 days following initiation of co-culture to monitor HaCaT cell growth. Representative experiment, n=2.

(**E**) Senescent BJ fibroblasts in matrigel were injected subcutaneously into the rear flanks of nude mice fed either control or p38i chow. Cells were removed 10 days after injection and IL8 mRNA levels were measured using qRT-PCR. Representative experiment, n=4.

(**F, G, and H**) Xenografts of BPH1-CBR cells co-injected with senescent BJ fibroblasts (SIPS) into female NcR nude mice. Control or the p38i compounded chow were performed as outlined in (**F**). Tumor are shown in (G). Tumor growth was analyzed by bioluminescence imaging (**H**). Data represent mean + SEM, n=8.

Data represent mean + SD unless otherwise stated. * indicates $p<0.05$. SIPS: stress induced premature senescence.

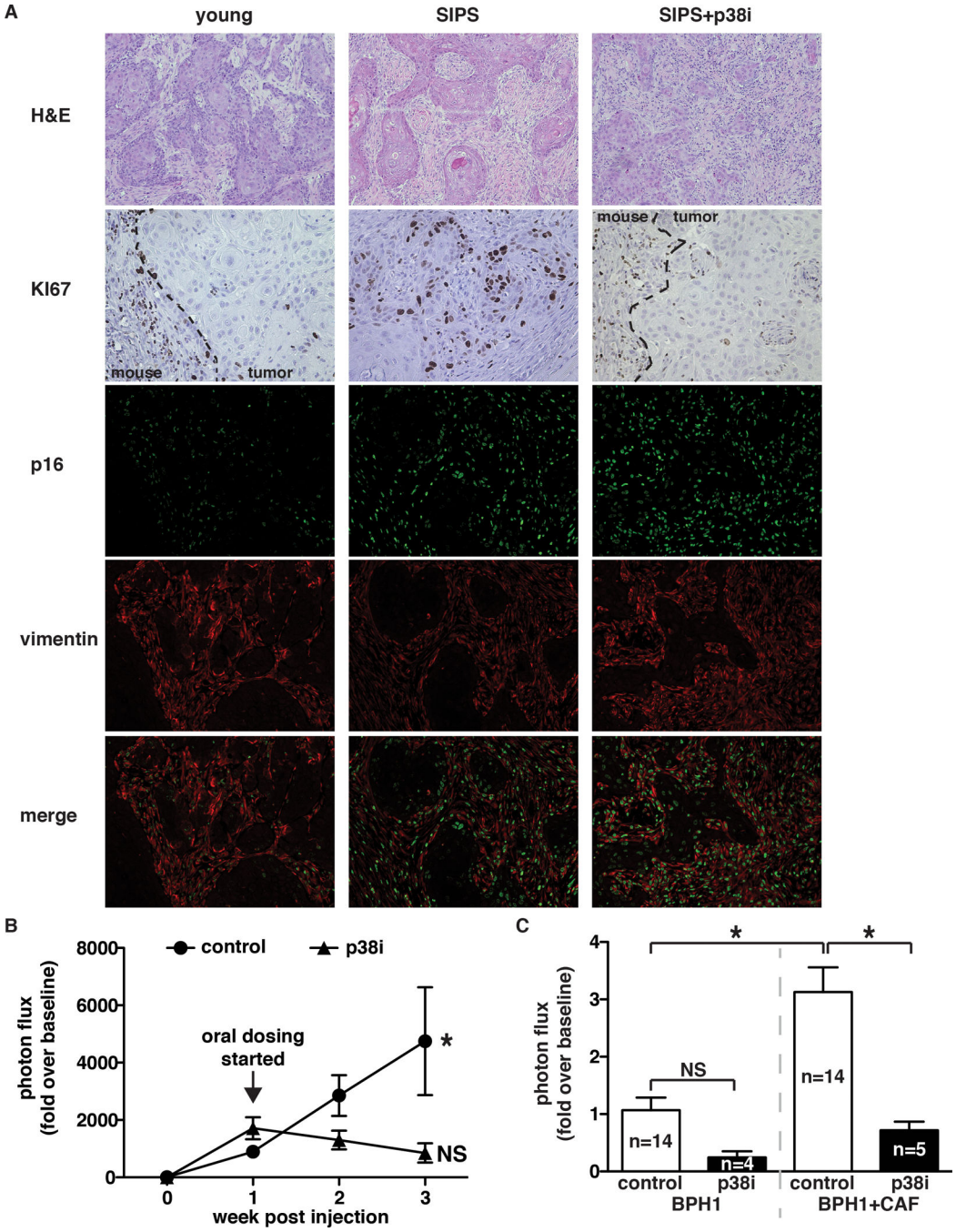

Fig 5. p38MAPK inhibition is effective in both senescent fibroblast and CAF-driven tumors

(**A**) Tumors were removed at the endpoint of the experiment described in (Fig 4F) and stained for Ki67 (dashed line demarks the margin between the mouse and xenograft), p16, and vimentin. H&E images were captured with a 10× objective, all other images were captured with a 20× objective. Representative images, n=2.

(**B**) Xenograft growth of BPH1-CBR cells co-injected with senescent BJ fibroblasts (SIPS) into female NcR nude mice. Tumors were allowed to grow for 1 week after injection, at which time mice were placed on control or p38i-compounded chow. Tumor growth was

analyzed by bioluminescence imaging. Data represent mean + SEM, n=16. * indicates significance between 1 and 3 weeks post-injection in mice fed control chow.
(**C**) Xenografts of BPH1-CBR cells co-injected with pCAFs into female NcR nude mice. Mice were fed control or p38i chow as outlined for the experiment in Fig 4F. Tumor growth was analyzed by bioluminescence imaging. Data represent mean + SEM, n is indicated for each sample.
* indicates $p<0.05$. NS: not significant.